Hindawi
Shock and Vibration
Volume 2022, Article ID 9824882, 12 pages
https://doi.org/10.1155/2022/9824882

Research Article

A Novel Damage Detection Method of Reinforced Concrete Frames Using Signal Processing and Extracted Near-Fault Fling-Step Pulses

Amir Ezzodin,[1] **Gholamreza Ghodrati Amiri**,[1] **Hosein Naderpour**,[2] **and Morteza Raissi Dehkordi**[1]

[1]*Natural Disasters Prevention Research Center, School of Civil Engineering, Iran University of Science & Technology, Tehran, Iran*
[2]*Faculty of Civil Engineering, Semnan University, Semnan, Iran*

Correspondence should be addressed to Gholamreza Ghodrati Amiri; ghodrati@iust.ac.ir

Received 24 February 2022; Revised 19 October 2022; Accepted 1 December 2022; Published 20 December 2022

Academic Editor: Zhaoye Qin

A new model-free output-only signal processing-based damage detection procedure was carried out in this paper. First of all, a finite element model as the representative of reinforced concrete (RC) frames was constructed and subjected to a specific loading protocol in OpenSees. The protocol consisted of 9 consequent different near-fault fling-step pulse-type earthquake records with low-amplitude white noises among them to simulate the collapse procedure. The analysis process was complemented in three levels: (a) the Fourier transform was utilized to extract the vibration frequency, (b) the time instants of damage occurrence were detected by using the discrete wavelet transform, and (c) accurate damage detection was made by using the extracted pulse components of the records as loading protocol for earthquake simulation and the discrete wavelet transform. The results revealed that the proposed combinatorial method could efficiently diagnose the damage in the RC frames. Also, applying a pulse component instead of an original record increases the accuracy of damage detection by 70%.

1. Introduction

Damage detection that determines damage localization and quantification in engineering structures is one of the significant parts of the structural health monitoring (SHM) procedure is damage detection. SHM systems have been categorized according to the type of information they provide and their sophistication level. The SHM systems' categorizations, exclusively instructive in perceiving the objectives of SHM, can be summarized as damage detection, damage localization, damage diagnosis, and damage prognosis, demonstrating how damage will develop and what will be the remaining life given the current damage state [1].

Various methods for structural damage identification have been developed. Grounded on the present correlation between the structure's physical properties and vibrational parameters, the majority of the recently proposed damage detection methods have aimed at employing the structures' vibrational properties for detecting damage. The occurrence of damage provokes several changes in the structures' physical properties that affect the vibrational properties.

Dimarogonas, known as one of the pioneers in structural damage identification, proposed a model in which the damage was considered a local flexibility; moreover, by employing fracture mechanics methods, Dimarogonas evaluated the equivalent [2]. To determine the damage in different structures, Chondros and Dimarogonas suggested methods by associating the intensity of the damage with the shifts in natural frequencies for the damage position being known [3].

Due to the precision of wavelet analysis in detecting localized perturbation in the mode shape caused by a crack presence, wavelet analysis has recently been recognized as a reliable tool for damage detection. Although wavelet transform's prominent advantages are owning effective localization features and not demanding the numerical

differentiation of measured data, its distinctive feature is that through an arbitrary resolution, the local characteristics in a signal can be detected [4, 5]. Crack identification in beams via wavelet analysis was investigated by Douka et al. [6]. Ovanesova and Suarez presented a study to determine the crack of frames and beams as well as their location through response signals from dynamic or static analysis [7].

Having integrated discrete and continuous wavelet transforms, Gökdağ and Kompaz presented a wavelet-based method to detect the damage of beam-typed structures assuming that the shape of the damage mode can consist of local damage-induced variations and an undamaged mode [8]. Bagheri et al. proposed a method to identify the vibration-based damage of plate structures through the curvelet transform [9] and employed their method in a rectangular plate, with four fixed supports, including one or two damages with desired location, length, and depth [9]. Through the 2D discrete wavelet transform, Bagheri et al. further presented a method to detect linear flaws in plate structures [10].

Aguirre et al. explored the practicality of employing output-only model-free wavelet-based techniques to identify damages in reinforced concrete structures under seismic loads [11]. To obtain the perturbation regarding the precise performance of the acceleration response in the bridge piers, a model-free output-only wavelet-based damage detection methodology was proposed by Naderpour et al. [12]. Employing a simplified numerical model and in situ vibration measurement enables some degrees of freedom. Having applied both continuous wavelet transform and extended finite element method, Pirboudaghi et al. suggested an approach to identify the seismic cracking of concrete dams [13]. Beheshti Aval et al., moreover, presented a signal-based seismic technique for structural health monitoring to detect damage and evaluate the severity of damage in a multistory frame under earthquake [14]. Babajanian Bisheh et al. proposed a new approach of detecting vibration-based damage given the selection of effective cepstral coefficients including the following three phases: (a) feature extraction and signal processing, (b) detection of damage by merging effective cepstral coefficients via methods of feature selection, and (c) performance evaluation. Given the adaptive feature extraction and signal processing [15], Babajanian Bisheh et al. further presented a novel approach for damage detection in a cable-stayed bridge [16]. Furthermore, Fallahian et al. also suggested an algorithm, which was assessed on the experimental data obtained from a large-scale bridge structure and a numerical model of a one-bay and three-story steel frame [17].

Owing to the reviewed literature, the differentiation between far-fault and near-fault earthquakes as well as the effect of pulse on the fault detection process has not been thoroughly addressed. Therefore, the current study was conducted aiming at employing a new output-only, wavelet-based damage detection method for predicting the damage occurrence in reinforced concrete frames subjected to near-fault fling-step pulse-type earthquake records. This study was conducted in three stages. In the first stage, the Fourier transform was applied to the time-history acceleration response of models in the white-noise range of the loading protocol, and the dominant vibration frequency of the structure was extracted. In the second stage, to identify the perturbation in the detailed decomposed function of the acceleration response, a discrete wavelet transform was employed due to the main record of the loading protocol. In the last stage, by using pulses extracted from near-fault earthquakes of loading protocol, the damage detection process was performed one more time and the difference between the responses due to the pulse effect and the effect of the main earthquake on the damage detection method was evaluated.

2. Signal Processing Method

Wavelet analysis has been considered to be one of the practical and efficient signal processing methods applied for structural health monitoring purposes [18, 19]. To assess the damage, nonstationary features of the structural response signal, including acceleration, have been employed by the wavelet tool. The Fourier transform is a powerful mathematical tool for obtaining the frequency components of a signal. The Fourier transform of a continuous time function is defined as follows:

$$X(f) = \int_{-\infty}^{+\infty} x(t).e^{-i2\pi ft}\mathrm{d}t. \quad (1)$$

Here, t and f are indicators of time and frequency, respectively.

One of the most important restrictions of the Fourier transform is that it only presents the existence or nonexistence of signal frequency content while not achieving the corresponding time interval of its occurrence, which is inefficient in signals which are nonstationary. Hence, for nonstationary signals, the windowed Fourier transform was used. In windowed Fourier transform, a signal is divided into short-enough parts, which are assumed to be stationary. In this case, the window function w is used, which has a length equal to the minimum required value for each signal part to be stationary. Consequently, for signal x (t) employing window w (t), the short-time Fourier transform would be as follows:

$$STFT_x^w(\tau, f) = \int_{-\infty}^{+\infty} x(t).w^*(t-\tau).e^{-i2\pi ft}\mathrm{d}t. \quad (2)$$

Here, f and τ are frequency and time variables, respectively. Since the time window length is variable in short-time Fourier transform, frequency and time resolutions should be taken into account. By increasing the time window length, good frequency and poor time resolution could be obtained. While, according to Heisenberg's uncertainty principle, by decreasing the time window length, inversed results would be obtained [20]. Multiresolution analysis was considered an alternative technique for signal processing used in the wavelet transform that has a resemblance, although with a dissimilar function, to the Fourier and

windowed Fourier transforms. The Fourier transform decomposed the signal into sine and cosine functions situated in the Fourier space. However, functions in both Fourier space and real space are employed in the wavelet transform. In general, the wavelet transform is an unlimited body of diverse functions that depends on the merit functions resulting in its application in a wide spectrum. In wavelet analysis, moreover, the similarity of a signal is compared with the mother wavelet function.

Function $\psi(x)$ is considered a wavelet given that its Fourier transform $\Psi(\omega)$ meets the following condition:

$$\int_{-\infty}^{+\infty} \frac{|\Psi(\omega)|^2}{|\omega|^2} d\omega < +\infty, \tag{3}$$

which could be summarized as follows:

$$\int_{-\infty}^{+\infty} \psi(x)\mathrm{d}x = 0. \tag{4}$$

Equation (4) implies a function with zero mean based on which many functions could be considered wavelet ones. $\Psi(x)$ is the mother wavelet function requiring shifting and/or scaling operators to influence the signal during analysis. Scaling a wavelet simply is stretching or compressing it, and shifting is delaying or hastening its onset. Equations (5) and (6) show the general state of the mother wavelet, including scaling and shifting capability, and continuous wavelet transform as the convolution of the signal and a shifted-scaled function of the wavelet, respectively.

$$\psi_{a,b}(x) = \frac{1}{\sqrt{a}}\psi\left(\frac{x-b}{a}\right), \tag{5}$$

$$C_{f,\psi}(a,b) = \frac{1}{\sqrt{a}}\int_{-\infty}^{+\infty} f(x).\psi^*\left(\frac{x-b}{a}\right)\mathrm{d}x. \tag{6}$$

Here, a and b present scaling and shifting factors and $\psi^*(x)$ is the wavelet function's complex conjugate.

Considering all possible scales would result in a huge number of calculations for wavelet coefficients, which is not necessary. A better way would be to select a subset of positions and scales. Many scholars have recommended positions and scales on the basis of the powers of the two, known as binary or dyadic positions and scales, by which the analysis obtained from the discrete wavelet transform is estimated to be more efficient and accurate [20–23]. The dyadic scaling and shifting parameters are shown in the equation:

$$a = 2^{-j}, b = 2^{-j}k. \tag{7}$$

Here, j and k are integers. By substituting equation (7) for equation (5), this could be found:

$$\psi_{j,k}(x) = 2^{(j/2)} * \psi\left(2^j k - k\right). \tag{8}$$

Discrete wavelet coefficients would then be as follows:

$$C_{f,\psi}(j,k) = \sum_{n\in Z} f(n).\psi_{j,k}(n). \tag{9}$$

Utilizing developed filters by Mallat is an efficient and classical technique in signal processing known as a two-channel subband coder [24]. Low-frequency content considers the most significant component of many signals giving an approximation of a signal and forming its identity. In contrast, the high-frequency content indicates the details of a signal.

Thus, reconstructing the signal would be possible by its approximation (A) and details (D) at diverse stages of decomposition (n) in the equation:

$$f(t) = A_n + \sum_{m\le n} D_n. \tag{10}$$

In the current study, the biorthogonal family, i.e., the *Bior6.8*, with the property of linear phase required for signal reconstruction (e.g., [7, 25, 26]), was employed for wavelet transforms. As it is demonstrated in Figure 1, by using two wavelets, one for decomposition and the other for reconstruction, as representatives of the main signal, considerable characteristics are obtained.

3. Finite Element Modeling and Earthquake Simulation

A reinforced concrete frame considered in this study was similar to the test specimen chosen for the experimental study by Hemmati et al. [28]. The moment-resisting frame with fixed supports was observed as a structural member, where time-history analysis and finite element modeling were carried on. The frame's clear span was 1200 mm, and the overall span was 1600 mm. The beams' cross section had a depth of 150 mm deep and a width of 200 mm. The frames' overall height was 1400 mm. Moreover, all columns' cross section had a depth of 200 mm and a width of 200 mm. Figure 2 demonstrates the view of the RC frame and its member section details.

Finite element models were created in the open system for earthquake engineering simulation called OpenSees [29], which is an object-oriented software framework used to stimulate the structural systems' seismic response. By applying a great variety of material models, solution algorithms, and elements, OpenSees maintains an exceptional capability for analyzing and modeling the nonlinear response of systems. To create structural models, the nonlinear beam-column displacement-based element having distributed plasticity in integration points was used. Integration through element length was based on Gauss–Lobatto quadrature points. The number of integration points was considered to be equal to 10. The fiber section method was further specified to determine the plasticity in integration points.

Being a general geometric configuration, a fiber section is composed of subregions with simpler regular forms, such as triangular, circular, and quadrilateral regions, called patches. Furthermore, it is feasible to determine the

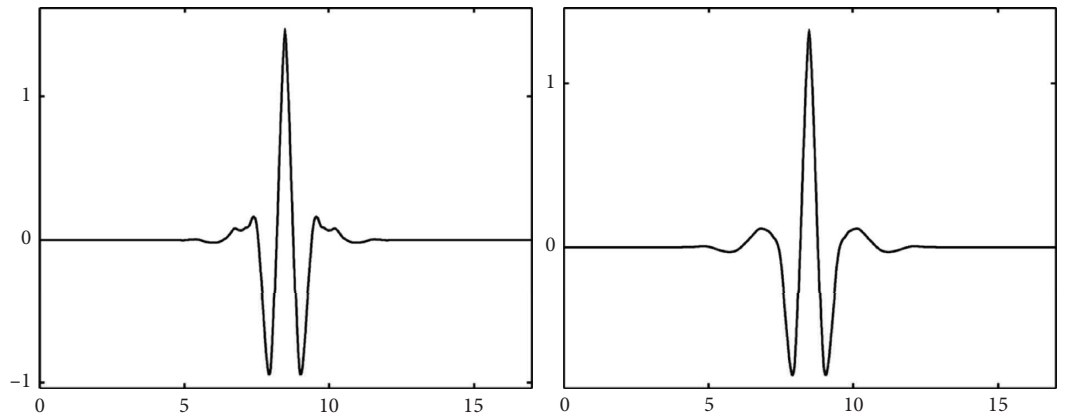

Figure 1: Mother wavelet function Bior6.8 for decomposition (a) and for reconstruction (b) [27].

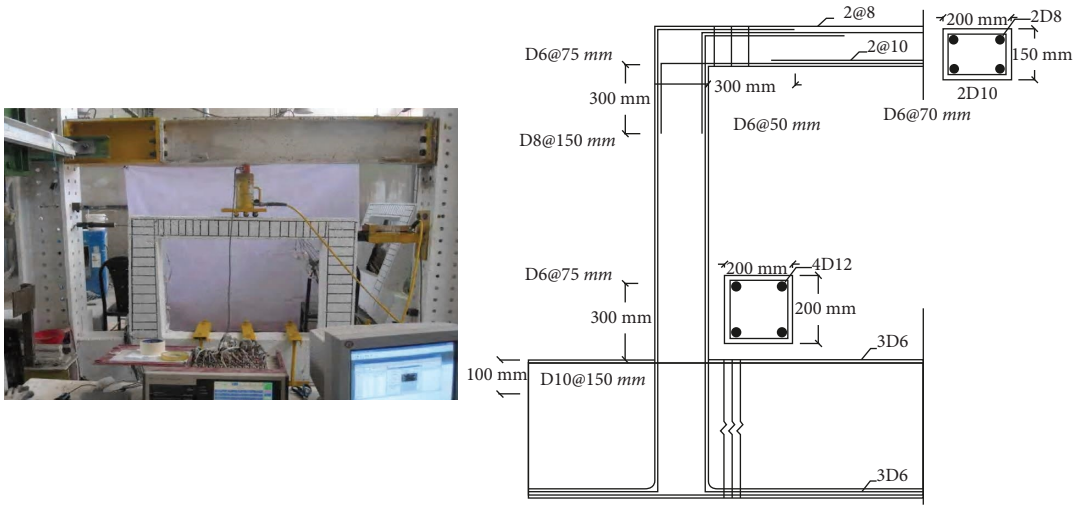

Figure 2: A view of the considered RC frame and details of the reinforcement layout of the frame [28].

reinforcement bar layers. The layer and patch subcommands were employed to outline the section into fiber discretization. Besides, individual fibers can be specified via the fiber command (fiber objects were linked to uniaxial material objects throughout the generation) enforcing assumptions of the Bernoulli beam. The uniaxial material, according to Mander et al., comprises *Concrete01* [30]; *ReinforcingSteel* is driven from [31]. Grounded on the Coffin–Manson fatigue model, degrading the strength and stiffness of the steel in cyclic loads was also addressed, and the related parameters are indicated in Table 1. Taking cyclic degradation into account, two factors, including C_f and α, were employed to correlate the number of the fracture's half-cycles with the plastic strain amplitude of the half-cycle (Figure 3). Taking into account the second-order effects of P-delta, a coordinate transformation was conducted with a linear geometric transformation of element stiffness and resisting force from the local to the global system.

A damping matrix was further determined as a combination of mass-proportional damping matrices and stiffness to attribute damping to the specified nodes and elements. For the models, a damping ratio of 5% was considered. As shown in Figure 4, regarding RC frames, the column and beam are divided into 15 and 16 elements, respectively. The mechanical properties of materials used in structural models are summarized in Table 2.

Table 1: Fatigue parameters.

Parameter	Definition	Considered value
α	Damage strain range constant	0.505
C_f	Ductility constant	0.187
C_d	Strength reduction constant	0.357

Since the number of integration points for each element was assumed to be 10, the numbers of integration points for each column and beam were 150 and 160, respectively.

To validate the finite element model, the lateral load-displacement curves of the experimental and numerical models are demonstrated in Figure 5. As it is shown in Figure 5, there is acceptable compatibility between experimental and numerical results.

Ground motion records (Table 3) beginning from low PGA values with constant growth up to the last one and enabling the simulation of the collapse procedure were also performed.

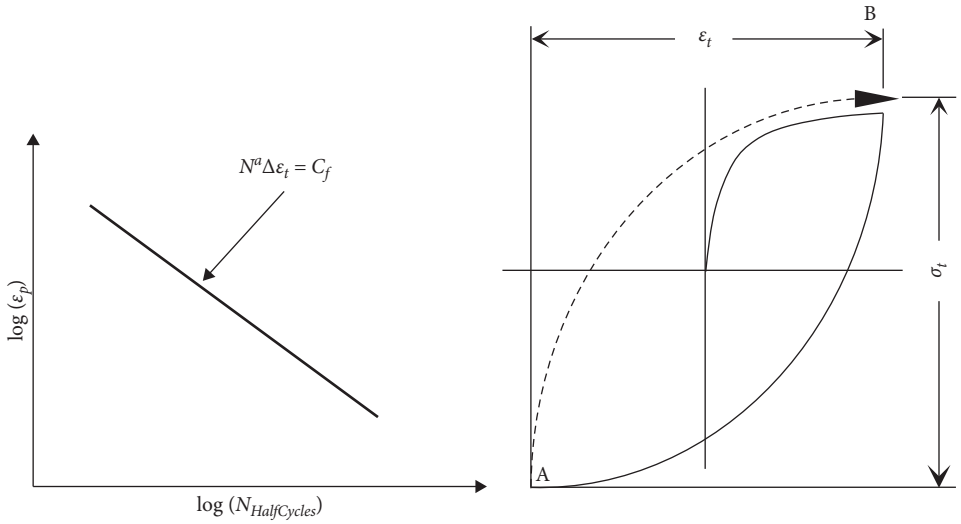

ε_p = half cycle plastic strain amplitude
ε_t = total half cycle strain amplitude
σ_t = total half cycle stress amplitude

Figure 3: Coffin–Manson constant (a) and half-cycle terms defined (b) [31].

Table 2: Materials properties.

Reinforcement (MPa)		Concrete (MPa)	
f_y	400	f'_c	48
f_u	600	f_{cu}	34.5
E_s	200000	E_c	20000

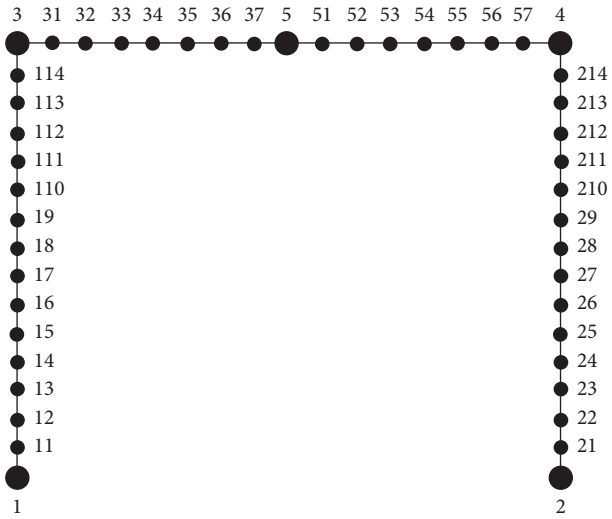

Figure 4: Finite element model.

To obtain every single record's dynamic feature and specific frequency component as well as maintaining the dynamic features regarding the structure after the completion of records, a low-amplitude white noise was employed both before and after each record.

A fling-step ground motion is mostly identified by an everlasting displacement in the time history of its displacement and a one-sided pulse in the time history of its velocity. The one-sided pulse in the time history of its velocity exists in a specific time window, in which the ground is subjected to an everlasting displacement in the time history of its displacement.

Several studies (e.g., [32–38]) have simulated the near-fault velocity pulse. In the present study, however, the fling-step pulse suggested by Ezzodin et al. [38] and the extracted pulse by using wavelet transform were utilized to analyze the effect of the near-fault pulse on the damage detection procedure.

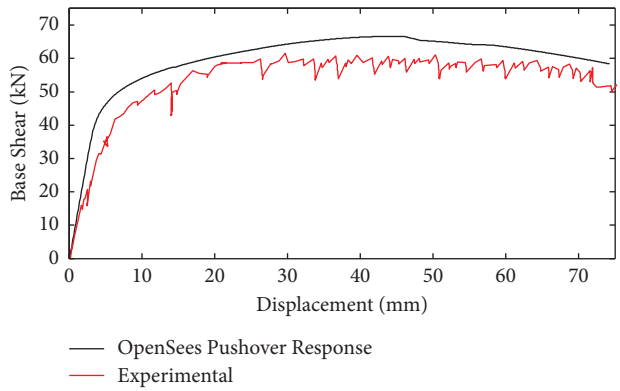

Figure 5: Comparison of numerical and experimental results.

Table 3: General information of ground motions used in loading protocol.

Record no	Year	Earthquake	MW	Station	Component	Dist. (km)	PGA (g)	PGV (cm/s)
1	1999	Chi-Chi	7.6	TCU082	EW	4.47	0.22	50.49
2	1999	Chi-Chi	7.6	TCU049	EW	3.27	0.27	54.79
3	1999	Chi-Chi	7.6	TCU075	EW	3.38	0.32	111.79
4	1999	Chi-Chi	7.6	TCU089	EW	8.33	0.34	44.43
5	1999	Chi-Chi	7.6	TCU052	EW	1.84	0.35	178
6	1999	Chi-Chi	7.6	TCU068	NS	3.01	0.36	294.14
7	1999	Kocaeli	7.4	Sakarya	EW	3.2	0.41	82.05
8	1999	Chi-Chi	7.6	TCU052	NS	1.84	0.4385	216
9	1999	Chi-Chi	7.6	TCU068	EW	3.01	0.5	277.56

It should be noted that the damage caused by each record was taken into account at the starting point of the following ground motion. Table 3 indicates the details of the utilized records. The acceleration component of the considered earthquake records, the pulse extracted by Ezzodin et al. [38], and the pulse extracted by using the wavelet transform are demonstrated in Figure 6. In addition, Figure 7 shows all 9 records with white noises.

4. Damage Detection in the Model

To detect damage, it was essential to determine the structural response of models. Figure 8 shows the acceleration response of the top point of the frame subjected to the loading protocol in Figure 7. Moreover, deriving from the records in Figure 7, each time-history response in Figure 8 shows a particular segment of the global acceleration response of the entire structure. As it is depicted in Figure 8, there is a gradual increase in the maximum acceleration of models due to the employed records. Before decomposing the structural response by wavelet, it is required to gain a proper understanding of the signal characteristics, such as the vibration frequency. Figure 9 presents the Fourier spectrum of the acceleration response as a result of a low-amplitude white noise observed both before and after each record.

When the damage occurred, stiffness decreased; consequently, the vibration frequency was affected. During an earthquake, everlasting structural stiffness loss occurs through a damaging process. A decrease in the fundamental frequency was also observed. Indicating this change in frequency, the Fourier spectrum of the acceleration response was also analyzed according to the employed white noises both before and after every record (Figure 10).

In this stage, structural damage was detected, and no further information regarding the damage was reported. Identifying the occurrence time of damage, the discrete wavelet transform that decomposed the response into two distinct components was applied to the acceleration response of the model regarding the 9 main near-fault records. A limited number of spikes were obtained from the high-frequency segment of the signal. By examining the detail function driven from a discrete wavelet transform, some irregularities were detected in the structure's high-frequency response. A sudden change in stiffness, by the failure of the rebar or large inelastic strains, would be reflected in the high-frequency component of the structure's acceleration response. A threshold criterion was further introduced by Aguirre et al. [11] to avoid the identification of false spikes. The details were transformed into standard ones using the equation:

$$z_i = \frac{D_i - \mu_D}{\sigma_D}, \tag{11}$$

where μ_D is the mean and σ_D is the standard deviation of the available details.

A significant number of points with more irregularities become evident by standardizing data; therefore, a threshold was taken into account to remove the lower points. Instants with a standard value of less than four, being equal to details with an absolute amplitude of deviation greater than $4\sigma_D$

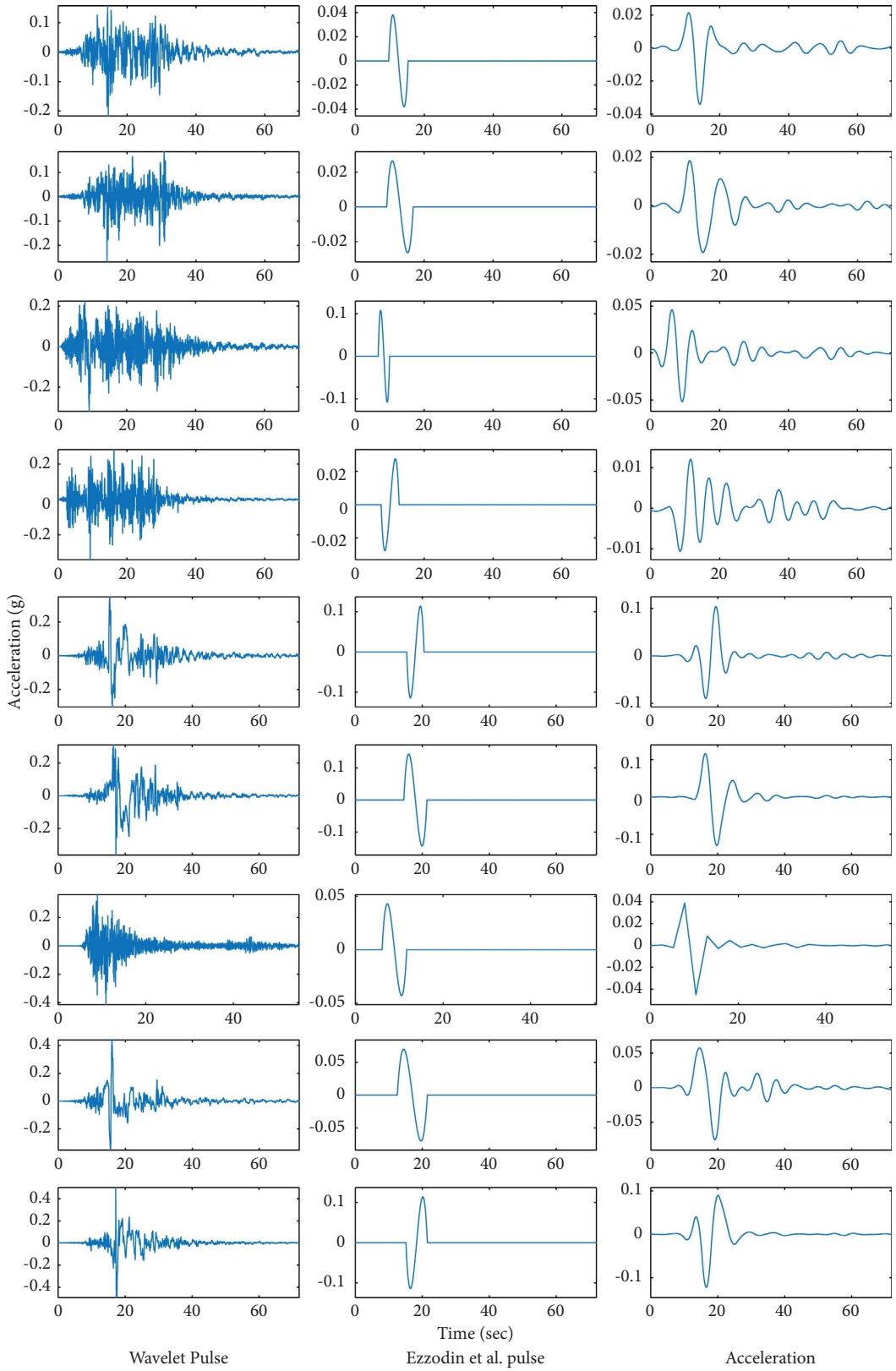

Figure 6: Acceleration components and extracted pulses.

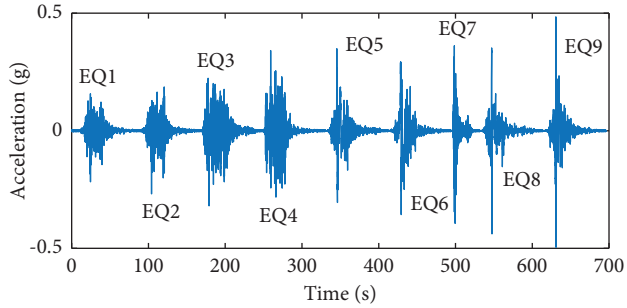

Figure 7: Loading protocol.

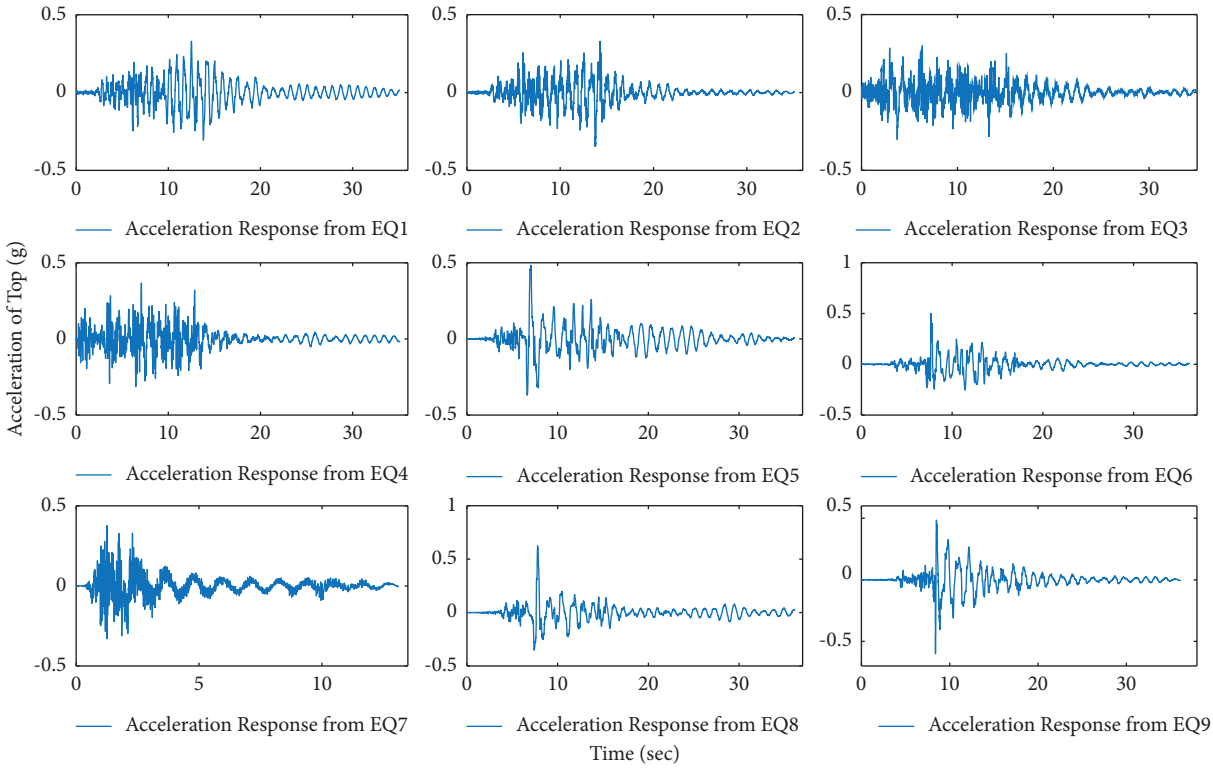

Figure 8: Acceleration response of the structure due to all records of loading protocol.

from μ_D, were determined as damage points. Thus, the confidence level of more than 95% was guaranteed. Given the aforementioned procedure, Figure 11 demonstrates the set of results obtained.

As demonstrated in Figure 11, some irregularities emerged indicating the occurrence of damage in the frame due to records. However, since there was no concentration on the irregularities, especially in earthquakes 4 to 9, it would be impossible to diagnose the damage. Therefore, considering that the pulses were the main components of the records and had almost all the main features of the records, accurate damage detection could be made. According to Figure 12, after the first earthquake, almost no damage occurred in the structure, while in Figure 11, after the first earthquake, the structure's damage was reported incorrectly. It could be inferred that there were various irregularities since various records did not have a particular sequence; hence, the severity of damage would be difficult to handle. Moreover, Figure 12 shows the concentration of irregularities, especially on earthquake records 6 to 9, where damage intensity of the reinforced concrete frame can also be obtained.

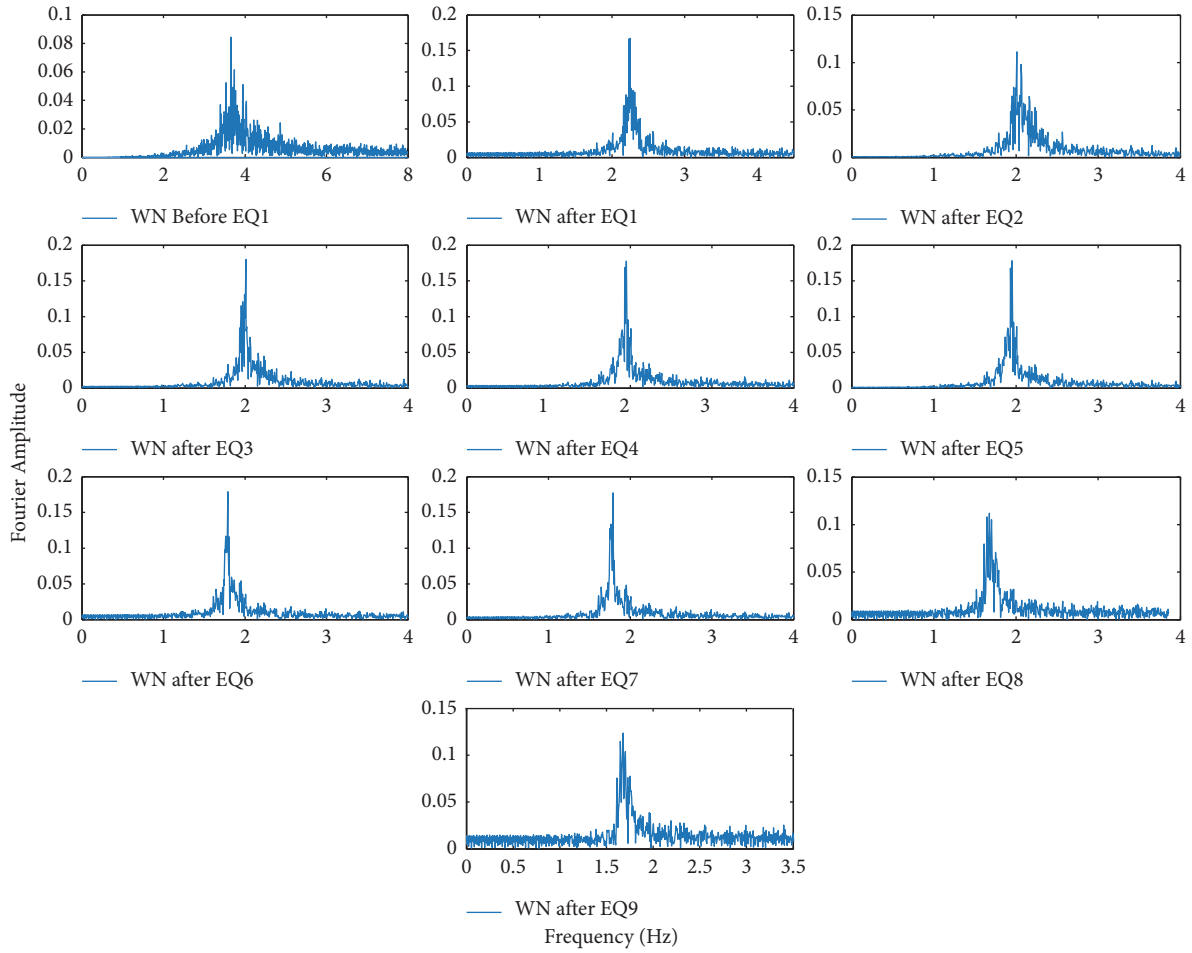

Figure 9: Fourier spectrum before and after each record.

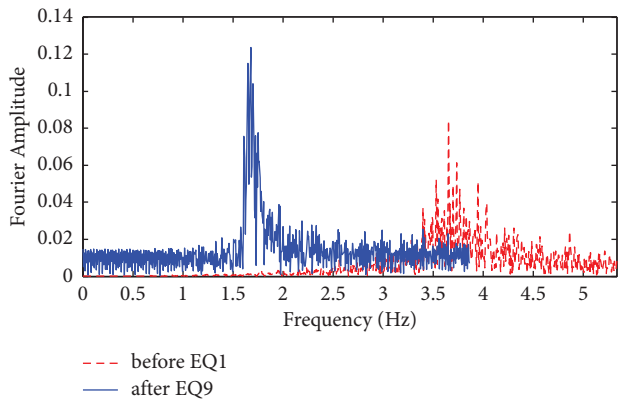

Figure 10: Fourier spectra before first and after last record.

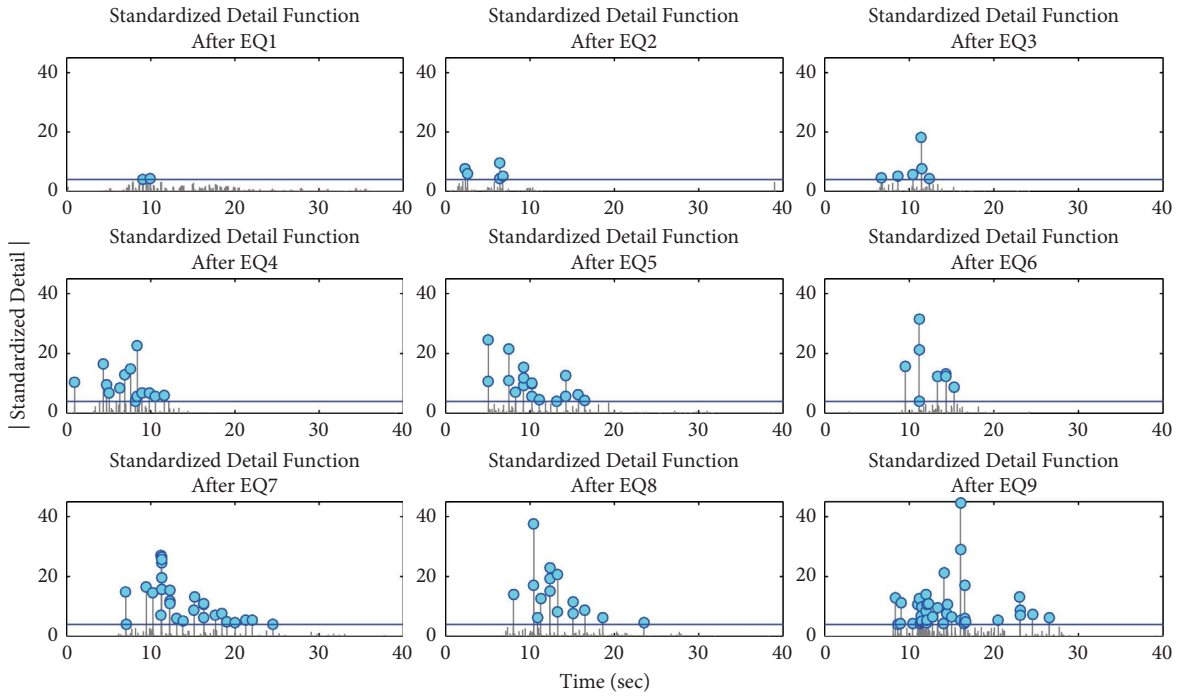

Figure 11: Standardized decomposed details of acceleration response due to all records.

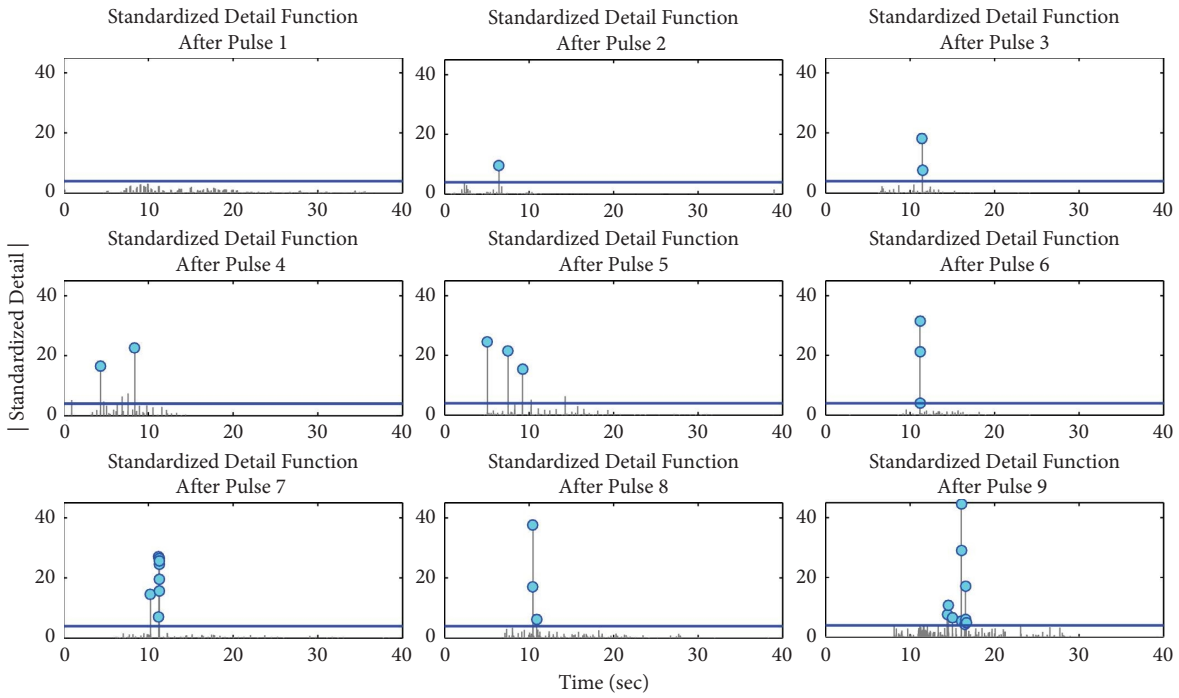

Figure 12: Standardized decomposed details of acceleration response due to all pulses.

5. Conclusions

A reinforced concrete frame was considered as the structural model, on which nonlinear time-history finite element analysis was carried out. Having gradual damage in models, a selected loading protocol consisted of 9 fling-step near-fault pulse-type subsequent records beginning from the low PGA values with constant growth up to the last one and providing the possibility of simulation of the collapse procedure was also applied. Three phases of analysis were considered for the damage detection of models. In the first phase, the Fourier transform was employed to achieve the dominant vibration frequency of the RC frame. The results revealed that by gradual application of excitations, the

frequency shifted considerably, implying damage existence. To detect the time of the occurrence of damage, a discrete wavelet transform was utilized in the second phase. By analyzing the detail functions obtained via the discrete wavelet transform, the time instant when the primary significant inelastic excursion took place was identified. Some irregularities in decomposed detailed response were reported, indicating damage occurrence in models based on the main part of the loading protocol. To avoid spurious spikes' identification, a threshold was chosen after standardizing data. The threshold made it feasible to eliminate the spikes' lower values. The rest of the points represented the episodes of damage. Perturbation's peak values were accounted to be the most effectual time instants of damage. Finally, regarding the innovation of the present study, by taking into account that the dominant pulse of the earthquake record could represent the main characteristics of the earthquakes, the loading protocol consisted of 9 extracted pulse components of the near-fault records which were investigated, and earthquake simulation was performed. The detailed functions obtained via the discrete wavelet transform were analyzed, and more concentrated spikes were observed, confirming the damage detection accuracy to more than 70 percent.

Data Availability

The data used to support the findings of this study are not available due to ethical restrictions.

Conflicts of Interest

The authors declare that they have no conflicts of interest.

References

[1] B. Gunes and O. Gunes, "Vibration-based damage evaluation of a reinforced concrete frame subjected to cyclic pushover testing," *Shock and Vibration*, vol. 2021, Article ID 6666702, 16 pages, 2021.

[2] A. D. Dimarogonas, *Vibration Engineering*, West Publishing Company, Saint Paul, MN, USA, 1976.

[3] T. G. Chondros and A. D. Dimarogonas, "Identification of cracks in welded joints of complex structures," *Journal of Sound and Vibration*, vol. 69, no. 4, pp. 531–538, 1980.

[4] D. E. Newland, "Wavelet analysis of vibration: Part 1—theory," *Journal of Vibration and Acoustics*, vol. 116, no. 4, pp. 409–416, 1994.

[5] D. E. Newland, "Wavelet analysis of vibration: Part 2—wavelet maps," *Journal of Vibration and Acoustics*, vol. 116, no. 4, pp. 417–425, 1994.

[6] E. Douka, S. Loutridis, and A. Trochidis, "Crack identification in beams using wavelet analysis," *International Journal of Solids and Structures*, vol. 40, no. 13–14, pp. 3557–3569, 2003.

[7] A. V. Ovanesova and L. E. Suárez, "Applications of wavelet transforms to damage detection in frame structures," *Engineering Structures*, vol. 26, no. 1, pp. 39–49, Jan. 2004.

[8] H. Gökdağ and O. Kopmaz, "A new damage detection approach for beam-type structures based on the combination of continuous and discrete wavelet transforms," *Journal of Sound and Vibration*, vol. 324, no. 3–5, pp. 1158–1180, 2009.

[9] A. Bagheri, G. Ghodrati Amiri, and S. A. Seyed Razzaghi, "Vibration-based damage identification of plate structures via curvelet transform," *Journal of Sound and Vibration*, vol. 327, no. 3–5, pp. 593–603, 2009.

[10] A. Bagheri, G. Ghodrati Amiri, M. Khorasani, and H. Bakhshi, "Structural damage identification of plates based on modal data using 2D discrete wavelet transform," *Structural Engineering & Mechanics*, vol. 40, no. 1, pp. 13–28, 2011.

[11] D. A. Aguirre, C. A. Gaviria, and L. A. Montejo, "Wavelet-based damage detection in reinforced concrete structures subjected to seismic excitations," *Journal of Earthquake Engineering*, vol. 17, no. 8, pp. 1103–1125, 2013.

[12] H. Naderpour, A. Ezzodin, A. Kheyroddin, and G. Ghodrati Amiri, "Signal processing based damage detection of concrete bridge piers subjected to consequent excitations," *Journal of Vibroengineering*, vol. 19, no. 3, pp. 2080–2089, 2017.

[13] S. Pirboudaghi, R. Tarinejad, and M. T. Alami, "Damage detection based on system identification of concrete dams using an extended finite element–wavelet transform coupled procedure," *Journal of Vibration and Control*, vol. 24, no. 18, pp. 4226–4246, 2018.

[14] S. B. Beheshti Aval, V. Ahmadian, M. Maldar, and E. Darvishan, "Damage detection of structures using signal processing and artificial neural networks," *Advances in Structural Engineering*, vol. 23, no. 5, pp. 884–897, 2020.

[15] H. Babajanian Bisheh, G. Ghodrati Amiri, M. Nekooei, and E. Darvishan, "Damage detection of bridges based on combining efficient cepstral coefficients," *Journal of Vibration and Control*, vol. 27, no. 19–20, pp. 2279–2290, 2021.

[16] H. Babajanian Bisheh, G. Ghodrati Amiri, M. Nekooei, and E. Darvishan, "Damage detection of a cable-stayed bridge based on combining effective intrinsic mode functions of empirical mode decomposition using the feature selection technique," *Inverse Problems in Science and Engineering*, vol. 29, no. 6, pp. 861–881, 2021.

[17] M. Fallahian, E. Ahmadi, and F. Khoshnoudian, "A structural damage detection algorithm based on discrete wavelet transform and ensemble pattern recognition models," *Journal of Civil Structural Health Monitoring*, vol. 12, no. 2, pp. 323–338, 2022.

[18] S. Beskhyroun, T. Oshima, and S. Mikami, "Wavelet-based technique for structural damage detection," *Structural Control and Health Monitoring*, 2009.

[19] T. Oshima, Y. Miyamori, S. Mikami, T. Yamazaki, S. Beskhyroun, and M. F. Kopacz, "Small damage detection of real steel bridge by using local excitation method," *Journal of Civil Structural Health Monitoring*, vol. 3, no. 4, pp. 307–315, 2013.

[20] S. Mallat, *A Wavelet Tour of Signal Processing the Sparse Way*, Academic Press, San Diego, CA, USA, 2009.

[21] I. Daubechies, "The wavelet transform, time-frequency localization and signal analysis," *IEEE Transactions on Information Theory*, vol. 36, no. 5, pp. 961–1005, 1990.

[22] C. Chui, *An Introduction to Wavelets*, Academic Press, San Diego, CA, USA, 1992.

[23] H. Stark, *Wavelets and Signal Processing an Application-Based Introduction*, Springer, Berlin Heidelberg, Germany, 2005.

[24] S. G. Mallat, "A theory for multiresolution signal decomposition: the wavelet representation," *IEEE Transactions on Pattern Analysis and Machine Intelligence*, vol. 11, no. 7, pp. 674–693, 1989.

[25] M. I. Todorovska and M. D. Trifunac, "Earthquake damage detection in the imperial county services building II: analysis

of novelties via wavelets," *Structural Control and Health Monitoring*, vol. 17, no. 8, pp. 895–917, 2010.

[26] L. A. Montejo, "Signal processing based damage detection in structures subjected to random excitations," *Structural Engineering & Mechanics*, vol. 40, no. 6, pp. 745–762, Dec. 2011.

[27] J. M. Misiti, Y. Misiti, G. Oppenheim, and M. Poggi, *Wavelet Toolbox for Use with MATLAB*, The Math Works, Inc, Hill Drive Natick, MA, USA, 2002.

[28] A. Hemmati, A. Kheyroddin, M. Sharbatdar, Y. Park, and A. Abolmaali, "Ductile behavior of high performance fiber reinforced cementitious composite (HPFRCC) frames," *Construction and Building Materials*, vol. 115, pp. 681–689, 2016.

[29] B. McKenna, G. L. Fenves, M. H. Scott, and F. Jeremic, "Open system for earthquake engineering simulation–opensees," 2000, http://opensees.berkeley.edu.

[30] J. B. Mander, M. J. N. Priestley, and R. Park, "Theoretical stress-strain model for confined concrete," *Journal of Structural Engineering*, vol. 114, no. 8, 1988.

[31] S. Mohle and J. Kunnath, "Reinforcing steel material," 2006, http://opensees.berkeley.edu.

[32] G. P. Mavroeidis and A. S. Papageorgiou, "A mathematical representation of near-fault ground motions," *Bulletin of the Seismological Society of America*, vol. 93, no. 3, pp. 1099–1131, 2003.

[33] S. R. Hoseini Vaez, M. K. Sharbatdar, G. Ghodrati Amiri, H. Naderpour, and A. Kheyroddin, "Dominant pulse simulation of near fault ground motions," *Earthquake Engineering and Engineering Vibration*, vol. 12, no. 2, pp. 267–278, 2013.

[34] K. K. Yadav and V. K. Gupta, "Near-fault fling-step ground motions: characteristics and simulation," *Soil Dynamics and Earthquake Engineering*, vol. 101, pp. 90–104, 2017.

[35] E. Kalkan and S. K. Kunnath, "Effects of fling step and forward directivity on seismic response of buildings," *Earthquake Spectra*, vol. 22, no. 2, pp. 367–390, 2006.

[36] H. Hamidi, H. Khosravi, and R. Soleimani, "Fling-step ground motions simulation using theoretical-based Green's function technique for structural analysis," *Soil Dynamics and Earthquake Engineering*, vol. 115, pp. 232–245, 2018.

[37] A. Ezzodin, G. Ghodrati Amiri, and M. Raissi Dehkordi, "A random vibration-based simulation model for nonlinear seismic assessment of steel structures subjected to fling-step ground motion records," *Journal of Vibration Engineering & Technologies*, vol. 10, pp. 2641–2655, 2022.

[38] A. Ezzodin, G. G. Amiri, and M. R. Dehkordi, "Simulation of fling step pulse of near-fault ground motion by using wavelet smoothening and improved bell-shaped function," *Soil Dynamics and Earthquake Engineering*, vol. 140, Article ID 106462, 2021.